Observations of Orographic Influences upon Large Scale Atmospheric Motions

by J. M. Wallace
Department of Atmospheric Sciences AK-40
University of Washington
Seattle, Washington 98195

1. Introduction

The forcing of flows by topographic features on the earth's surface gives rise to a wide range of phenomena in the atmosphere and oceans. Some of the more direct and obvious effects, such as mountain/valley winds,have probably been recognized since the dawn of civilization, while other more complex and subtle effects, such as gravity wave drag, are just now beginning to emerge in careful, statistical analyses of large data sets. Of all the subgrid-scale processes that have to be represented in numerical weather prediction models, the effects of terrain probably have the largest influence on performance. Despite the considerable progress of the past decade, a great deal of work still remains to be done to optimize the representation of terrain in these models.

In this observationally oriented discussion, I will consider the effects of terrain in the context of the zonally symmetric circulation, planetary waves, synoptic scale disturbances, and subsynoptic scale features in separate sections. In the first three of these sections I will divide the discussion into two parts: one dealing with the steady atmospheric response to the mountains and the second dealing with transient effects induced by mountains. The zonally symmetric circulation and planetary waves are of greatest relevance to extended range prediction, synoptic scale disturbances to the more conventional range of numerical weather prediction and subsynoptic scale features to short range prediction and to the interpretation of forecast charts in a local context.

2. The zonally symmetric flow

(a) The steady state response to mountains

The influence of mountains upon the climatological mean zonally symmetric circulation cannot be diagnosed directly because it represents the net result of a complex array of interactions between different physical processes. However, we can obtain some qualitative

insight into the nature of this influence simply by comparing the general circulation of the Northern and Southern Hemispheres. Of course, not all the differences that are evident in such a comparison can necessarily be directly attributed to the differences in orographic forcing in the two hemispheres, but I believe that there exists a broad consensus that the following differences are due to weaker orographic forcing in the Southern Hemisphere; i.e., none of the midlatitude Southern Hemisphere mountain ranges are comparable in height or areal extent to the Himalayas, and the Andes are not nearly as extensive as the Rockies in the latitude belt of the westerlies.

The Southern Hemisphere surface westerlies are almost twice as strong as their Northern Hemisphere counterparts in the 40°-60° latitude belt [e.g., see Oort (1983)]. This difference in surface wind speed is believed to be a reflection of the mechanisms that limit the buildup of westerly angular momentum in the extratropical atmosphere due to the poleward flux from the tropics in the two hemispheres. In the Northern Hemisphere mountain torques associated with the east-west pressure differences across the Rockies and Himalayas [e.g., see Newton (1971)] and gravity wave drag induced by these same ranges [e.g., see Palmer et al. (1986)] contribute to the removal of westerly momentum from the atmosphere, whereas in the Southern Hemisphere, the torque associated with the surface wind stress is the only effective removal process. Since the poleward eddy fluxes of angular momentum across 30° latitude are roughly comparable in the two hemispheres, it follows that the surface westerlies in the Southern Hemisphere must be stronger in order to remove, by surface wind stress alone, as much angular momentum as is removed through the combination of the three different processes in the Northern Hemisphere.

The difference in orographically induced gravity wave drag is believed to be responsible for the stronger wintertime westerlies in the Southern Hemisphere stratosphere and mesosphere. In the presence of these stronger winds, planetary waves do not propagate as readily from the troposphere into the stratosphere to produce midwinter warmings [Charney and Drazin (1961)]. Hence, the Southern Hemisphere wintertime polar vortex is more quiescent and less variable from year to year.

In retrospect, it appears that the tendency for excessively strong westerly winds that has been evident in virtually all the high resolution general circulation models until the past few years is a reflection of the relatively weak orography in these models. It appears that this bias can be corrected by a suitable combination of enhanced orography and gravity wave drag [Wallace et al (1983), Palmer et al. (1986)].

(b) Transient influences

The torque that the Northern Hemisphere mountains exert on the atmosphere is by no means steady, as evidenced by the contrasting sea-level pressure patterns in Fig. 1 which shows composite maps corresponding to strong and weak zonally averaged geostrophic surface

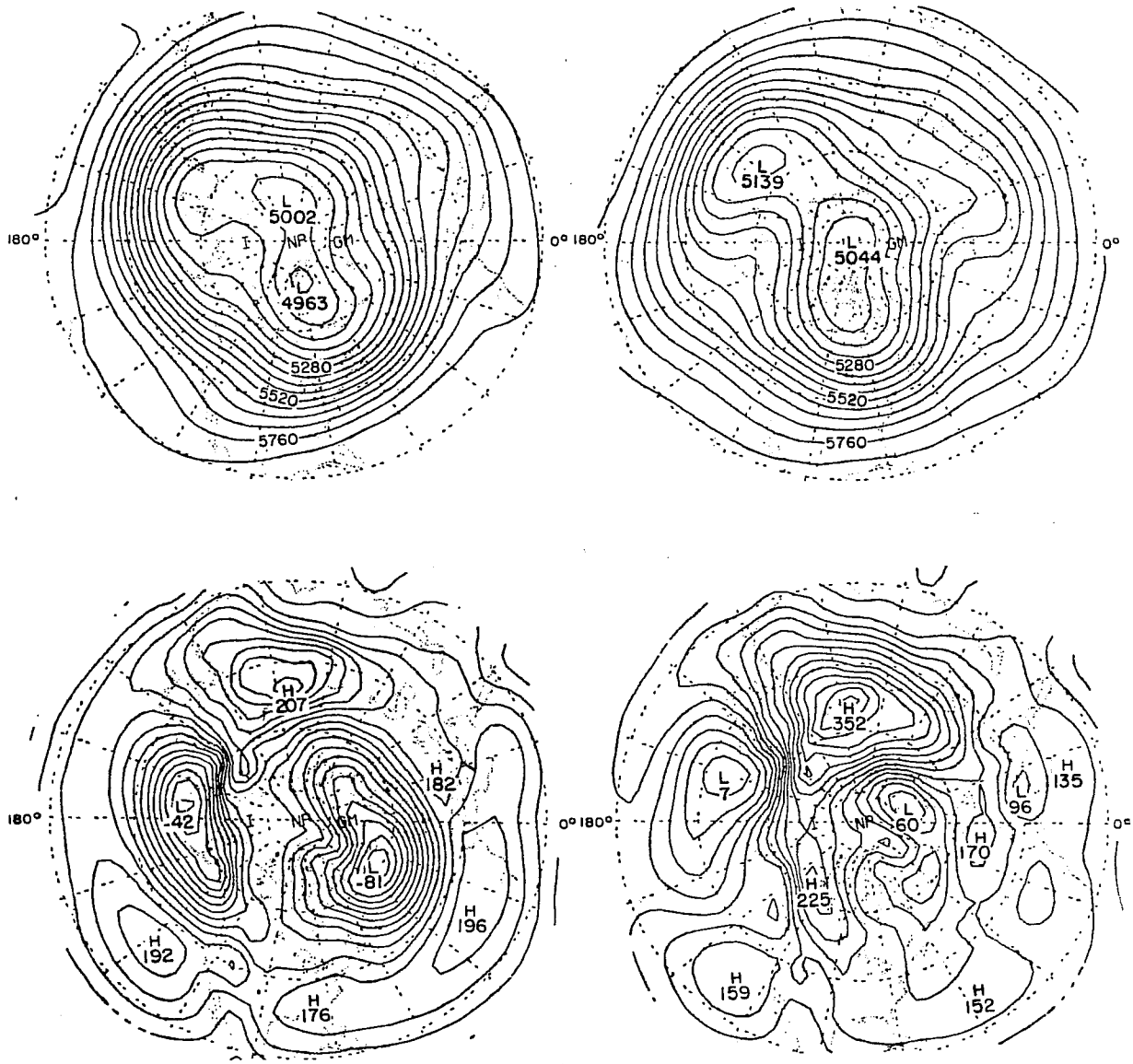

FIG.1. Composite maps illustrating the circulation patterns during high and low zonal index conditions during the Northern Hemisphere winter. The zonal index is based on the zonally averaged sea-level pressure difference between 35°N and 55°N in 5-day mean charts. Upper panels are 500mb charts, contour interval 60m; lower panels are 1000mb height charts, contour interval 30m. labels in mb and tenths minus 1000mb: left-hand panels show high index conditions (strong westerlies); right-hand panels show low index conditions (weak westerlies). For further details see Wallace and Hsu (1985).

winds in the 30°N-50°N latitude belt. The index used in generating these composite maps is similar to the one used by Rossby (1939) and collaborators in their studies of the index cycle phenomenon. In the strong westerlies composite (lower left) sea-level pressures are higher on the west side of the Rockies than on the east side and therefore the atmosphere may be viewed as pushing eastward on the Rockies, thereby giving up angular momentum to the solid earth. In the contrasting weak westerlies composite (lower right), pressure is higher along the east slopes of the Rockies, so the atmosphere is gaining angular momentum from the solid earth as a result of the mountain torque in this region. The differences between the two composites in the vicinity of the Himalayas are more subtle, but they are in the same sense. Hence, in a relative sense, the mountain torques extract angular momentum from the westerlies when they are stronger than normal, and feed angular momentum into the westerlies when they are weaker than normal. This negative feedback should tend to stabilize the strength of the zonally averaged westerlies. During strong cold air outbreaks, the fluctuations in the eastward mountain torque on the atmosphere may be much stronger than indicated in Fig. 1 [e.g., see Fig. 7], and the resulting acceleration of the zonal flow may be quite strong for periods of a few days.

The corresponding 500 mb charts shown in the upper panels of Fig. 1 exhibit marked differences in the planetary wave configuration, indicative of differences in the fluxes of angular momentum by the stationary waves. In the strong zonal wind composite (upper left) the trough/ridge configuration in the vicinity of the Rockies exhibits a distinctive NW/SE phase tilt poleward of 50°N and a NE/SW phase tilt around 30°N . This configuration is indicative of a convergence of westerly momentum flux by the stationary waves into the 30°-50°N latitude belt, which should have the effect of accelerating the westerlies. The slopes of the stationary waves in the weak zonal wind composite (upper right) are less prominent and therefore it seems reasonable to infer that the forcing of the zonal flow is weaker. The differences between the strong and weak wind composites in the vicinity of the Himalayas are in the same sense, but they are more subtle. Hence, it appears that there is a positive feedback between the stationary wave forcing and the mean zonal flow.

The interplay between mountain torques and stationary wave forcing can give rise to interesting low-frequency behavior in simplified models of the general circulation [e.g., see Charney and Devore (1979)]. Many of these models exhibit distinctive high and low index (i.e., strong and weak zonal wind) states, each with its own equilibrium stationary wave pattern induced by the orographic forcing. If this comcept of *multiple equilibria* is relevant to the atmosphere, one should expect to see two (or perhaps more) modes in the frequency distribution of zonally averaged zonal wind speed and in indices describing the hemispheric planetary wave configuration. Benzi et al. (1986) and Hansen (1986) have found evidence of bimodality in an index of stationary wave amplitude, but it does not appear to be

accompanied by a corresponding structure in the frequency distribution of zonal wind speed. Hence, at this point I am inclined to consider this fundamental question as unresolved.

3. Planetary waves

(a) Steady state response to mountains

The climatological mean stationary waves are well documented in the literature; for a review, see Wallace (1983). For the sake of illustration, the planetary scale upper level structure of the Northern Hemisphere wintertime stationary waves is documented in Figs. 2-3. It is evident from modelling studies of Grose and Hoskins (1979) and Held (1983) that planetary-scale wavetrains emanating from the Himalayas and Rockies are responsible for the

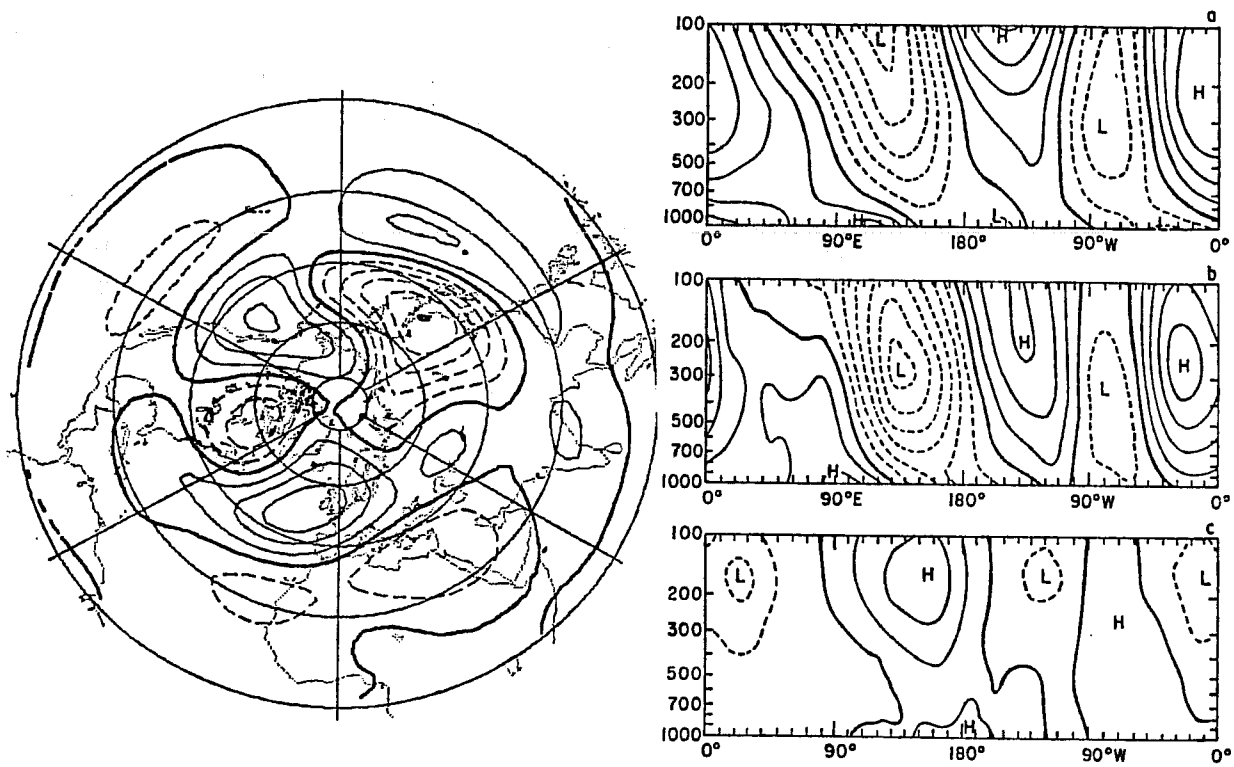

FIG.2. Northern Hemisphere climatological mean wintertime stationary waves. Left: 200mb geopotential height departures from their respective zonal mean values based on Crutcher and Meserve (1970); contour interval 60m; dashed contours denote negative values, zero contour is thickened. Right: zonal cross sections of geopotential height along 60°N (upper), 45°N (middle), and 25°N (lower); contour interval 50m, based on NMC analyses; dashed contours denote negative values. After Wallace (1983).

more prominent features in these patterns. These features exhibit only a small westward tilt with height and can be accurately simulated with simple barotropic models. In higher latitudes, troughs are situated poleward and downstream of both ranges. The longitudinal structure has been well understood theoretically dating back to the works of Charney and Eliassen (1949) and Bolin (1950) . However, the understanding of the two dimensional structure in Fig. 2a is a much more recent development. The NE/SW phase tilt of the features over Europe is a reflection of southeastward energy dispersion in this region and the tendency for subtropical features to be out of phase with those at higher latitudes is due to the reflection of the planetary-scale wavetrains from the tropics.

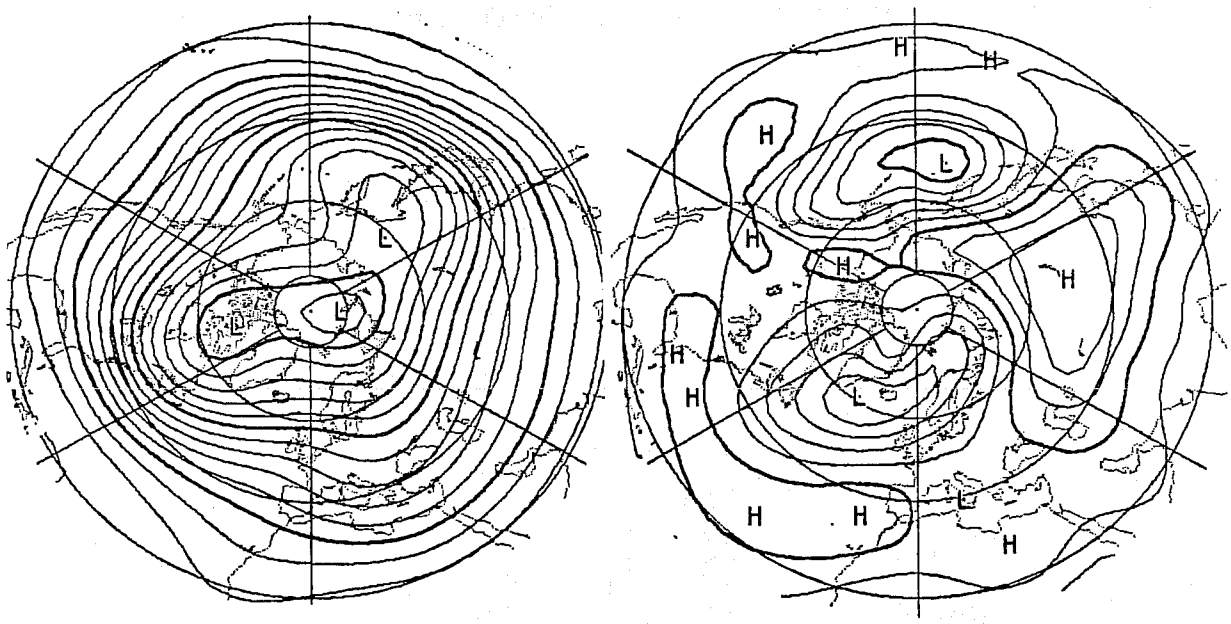

FIG.3. Northern Hemisphere climatological mean wintertime charts, based on NMC analyses. Left: 500mb height, contour interval 60m. Right: sea-level pressure, contour interval 4mb. After Wallace (1983).

Orographic forcing also appears to be responsible for two prominent planetary scale features in the wintertime climatological mean sea-level pressure pattern: the Siberian anticyclone and its extension across the Arctic to form a ridge of high pressure along the eastern slopes of the Rockies, as shown in Fig. 3b. These features are conspicuously absent in numerical simulations without mountains [Manabe and Terpstra (1974)] and they have tended to be too weak in models with standard orography. On the other hand, Maurice Blackmon and I have found that it is distressingly easy to generate 1080mb anticyclones in the lee of the Canadian Rockies by introducing envelope orography into the NCAR Community Climate Model.

The corresponding summertime planetary waves are weaker and shorter in wavelength, as illustrated in Fig.4. A prominent ridge is situated directly above the Rockies and there are indications of weaker ridges associated with other regions of high terrain. Hence, the phase relation between the planetary waves and the mountain ranges appears to be fundamentally different in the two seasons.

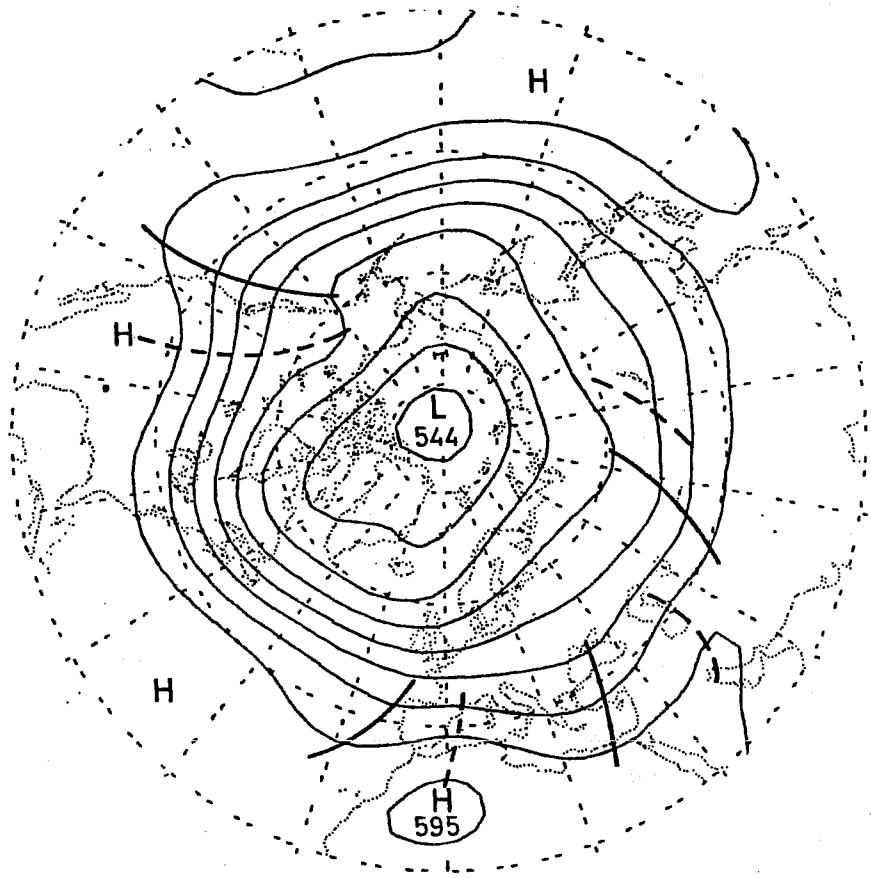

FIG.4. Northern Hemisphere climatological mean summertime 500mb height chart based on NMC data; contour interval 60m. After Wallace (1983).

b) Low-frequency signatures of mountains

Blackmon et al (1979) documented the existence of strong geographical contrasts in the vertical structure of low frequency atmospheric fluctuations about the climatological mean state. These contrasts are reflected in the correlation coefficient between 1000 and 500 mb height based on 5 day mean wintertime data shown in Fig.5. Over the oceanic sectors of the hemisphere and Europe the vertical structure exhibits a strong barotropic component, reflected in the high positive correlations between 1000 and 500 mb height. However, in narrow bands along the lee of the Rockies and to the north and east of the Tibetan Plateau, a much more baroclinic structure is observed, as reflected in the weak and even negative correlations in Fig.5. This rather complex pattern is simulated in general circulation models with a remarkable degree of fidelity: e.g., see Blackmon and Lau (1980).

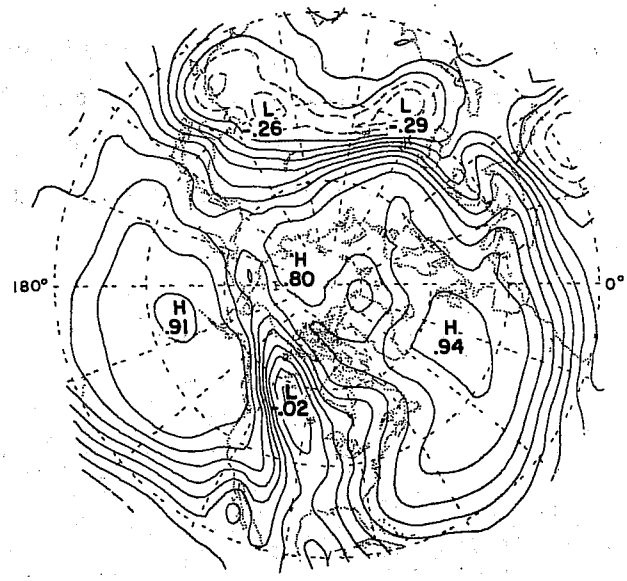

FIG.5. Local correlation between sea-level pressure and 500mb height in 5-day mean wintertime NMC analyses; contour interval 0.1, negative contours are dashed. Based on results in Blackmon et al. (1979) as recalculated in Hsu and Wallace (1985).

Hsu and Wallace (1985) have shown that the pattern in Fig.5 is a reflection of horizontal structures similar to the ones shown in Fig.6, which is a one point correlation map based on sea-level pressure in the Yukon. A number of significant features are evident in this pattern. The horizontal scale of the sea-level pressure fluctuations is larger than that of the corresponding 500 mb height fluctuations. Pressure in the Yukon is positively correlated with pressure in a band extending southeastward in the lee of the Rockies into the central U.S., roughly paralleling the region of weak correlations in Fig.5. There is a strong correlation gradient across the Rockies. To the west of the Rockies, the structures in the SLP and

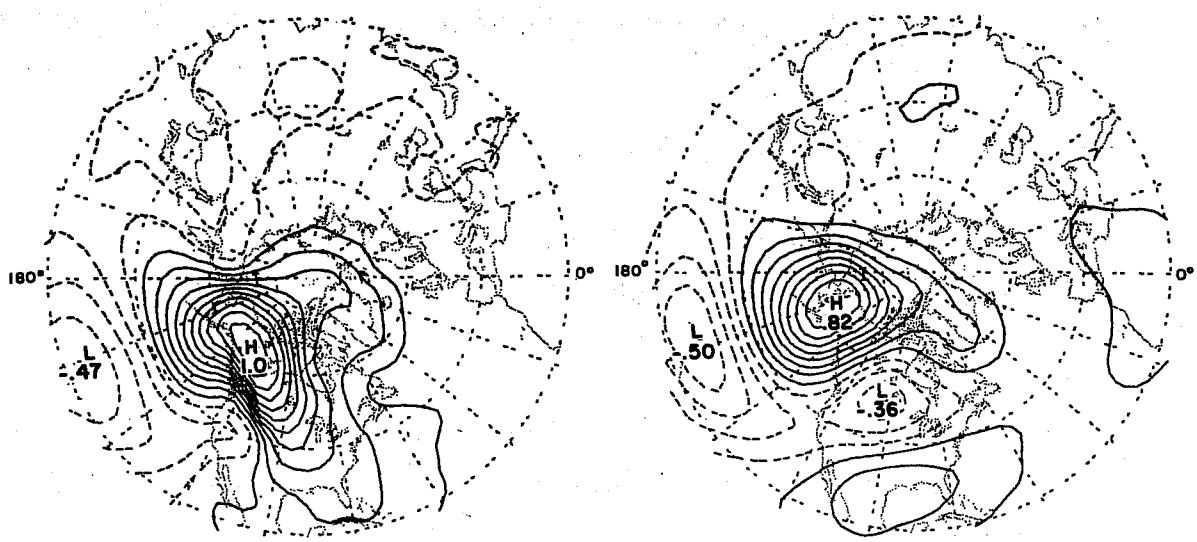

FIG.6. Simultaneous correlation between sea-level pressure at a gridpoint in the Yukon Territory and (left) hemispheric sea-level pressure and (right) hemispheric 500mb height. Based on 5-day mean, wintertime NMC analyses. Contour interval 0.1, negative contours are dashed. After Hsu and Wallace (1985).

500mb height fields are similar; in this region the pattern associated with pressure fluctuations in the Yukon tends to be quite barotropic, in agreement with Fig.5. However, to the north and east of the Rockies the sea-level pressure and 500 mb height patterns exhibit

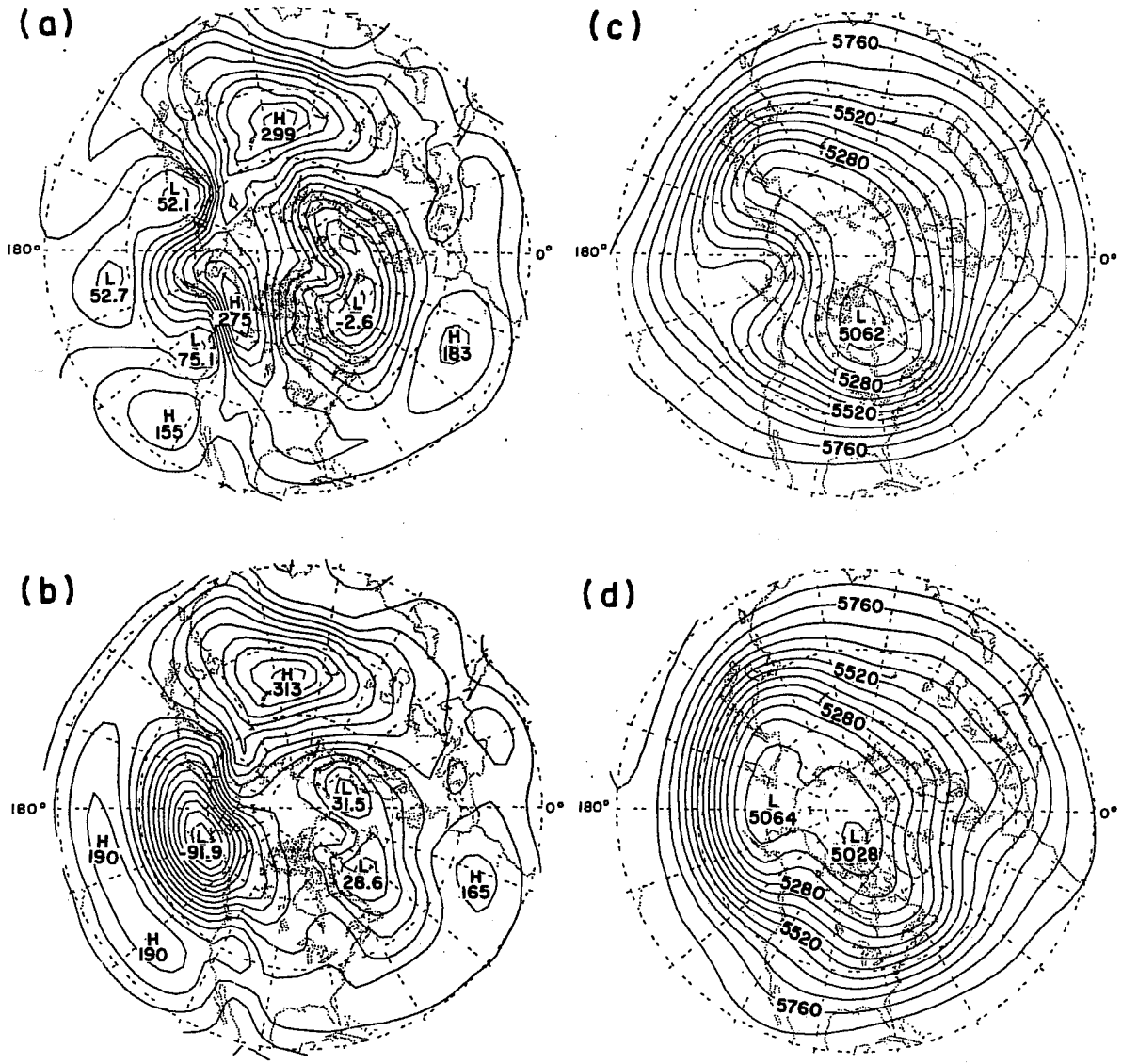

FIG.7. Composite sea-level pressure and 500mb height charts based on the orthogonally rotated principal component of the 5-day mean wintertime hemispheric NMC sea-level pressure analyses whose time series is closely related to pressure anomalies in the Yukon Territories. Left panels are sea-level pressure charts, contour interval 2mb, labels in mb and tenths minus 1000mb; right panels are 500mb charts, contour interval 60m. Upper panels correspond to high pressure in the Yukon; lower panels to low pressure in the Yukon. After Hsu and Wallace (1985).

different shapes and, within a large region centered over Montana, fluctuations at the two levels tend to have the opposite polarity. Similar patterns are observed for base gridpoints located farther southeast along the lee of the Rockies.

Fig.7 shows contrasting composite sea-level pressure and 500 mb height patterns based on an index which is very closely related to the Yukon pressure time series used in generating

Fig.6 [for further details, see Hsu and Wallace (1985)]. In the vicinity of the Rockies patterns similar to those in Fig. 1 are evident, but the features are accentuated. The pattern in Fig.7a can be interpreted as a reenforcement of the climatological mean ridge of high

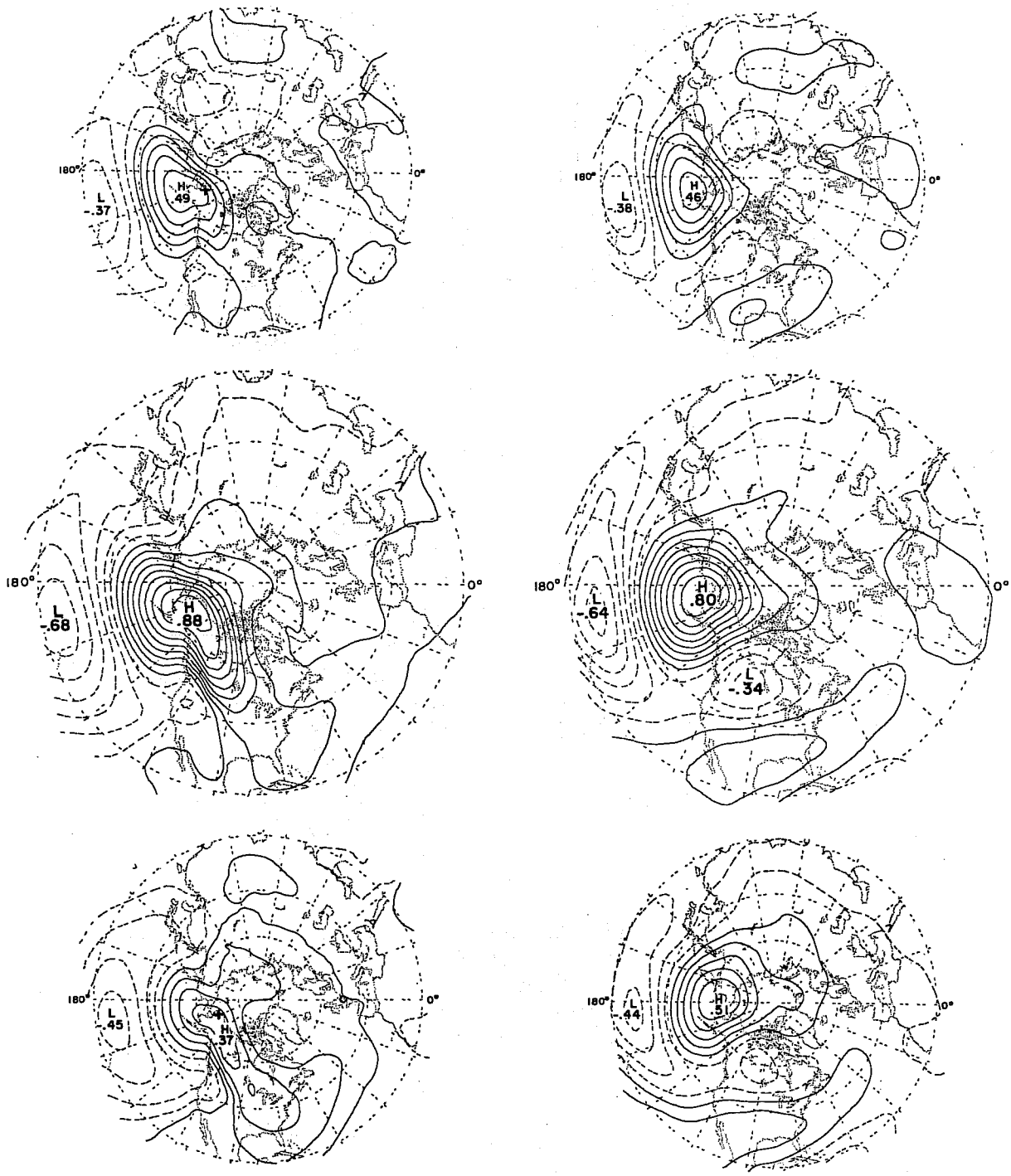

FIG.8. Lag correlation maps based on the orthogonally rotated principal component of the 5-day mean wintertime hemispheric NMC sea-level pressure analyses whose time series is closely related to pressure anomalies in the Yukon Territories. Left panels are sea-level pressure charts, right panels are 500mb charts, contour interval 0.1, dashed contours denote negative correlations. Upper panels show hemispheric patterns 5 days in advance of the reference timeseries; middle panels show simultaneous correlations with the reference timeseries (note the similarity to Fig.6); and lower panels show hemispheric patterns 5 days later than the reference timeseries. After Hsu and Wallace (1985).

pressure along the lee slopes of the Rockies. The contrasting pressure patterns in Figs.1 and 7 are reminiscent of the examples that appeared repeatedly in the index cycle literature of a generation ago [e.g., see Starr (1942), Willet (1944), Petterssen (1956)].

The nature of these patterns becomes more clearly evident when we examine their time evolution, as revealed by the lag-correlation maps shown in Fig.8. Note the apparent

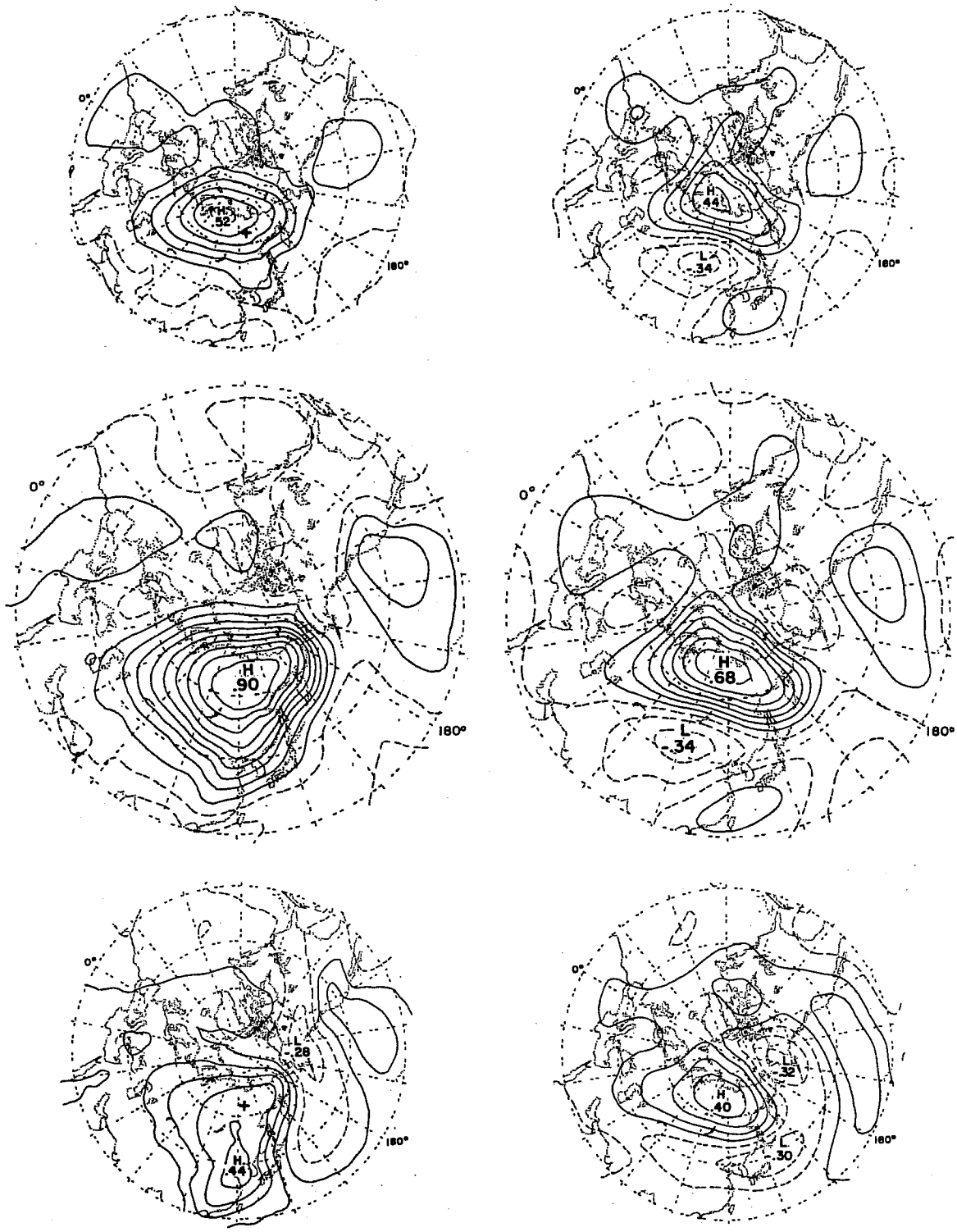

FIG.9. As in Fig.8, but for a Siberian gridpoint.

propagation and expansion of the region of positive correlations in the sea-level pressure field from Alaska, southeastward along the lee slopes of the Rockies. The evolution at the 500 mb level, shown in the right-hand panels, is entirely different: little phase propagation is evident, apart from the northwestward movement of the primary centre of action over the Gulf of Alaska. Some downstream energy dispersion is evident in the intensification of the wave pattern over North America during the sequence. The different pattern of evolution at the two levels transforms the vertical structure of the pattern from nearly barotropic early in the sequence (upper panels) to highly baroclinic late in the sequence (lower panels). Fig.9 shows corresponding results for a pattern related to sea-level pressure fluctuations over Siberia. In common with the results described above, we note the large horizontal scale and the southeastward propagation of the sea-level pressure pattern, the downstream energy dispersion at the 500 mb level, and the transformation of the vertical structure from barotropic early in the sequence to more barotropic later in the sequence.

Hence, the distinctive signature of mountain ranges in Fig.5 is inextricably linked to the tendency of sea-level pressure anomalies to be steered in a clockwise sense around the cold side of the major terrain features in the hemisphere. The behaviour is in marked contrast to the prevailing evolution of low-frequency patterns aloft, and at the earth's surface elsewhere in the hemisphere, which is dominated by downstream energy dispersion through wavetrains which exhibit little phase propagation [Blackmon et al., (1984)]. The low-level phase propagation along the topographic waveguides profoundly alters the vertical structure of low-frequency variability in these regions, such that sea-level pressure and upper tropospheric geopotential height fluctuations are often of opposite polarity.

4. Synoptic scale disturbances

(a) Steady state response

Fig.10, reproduced from Lau et al. (1981), shows the distribution of climatological mean vertically averaged (800, 700, 500 mb) relative vorticity in the lower troposphere during the winter season. Synoptic scale regions of anticyclonic relative vorticity are present over most of the major mountain complexes located poleward of the jetstream. (For a schematic depiction of the mountain ranges, see Fig.18). Particularly evident are the blobs of anticyclonic vorticity over Greenland, the Rockies, and the northernmost features of the Himalayan complex. It seems reasonable to interpret these features in terms of the conservation of potential vorticity in layers of air which temporarily contract in the vertical and spread out in the horizontal as they pass over these terrain features. Even more distinctive features would likely emerge in composite maps based on subsets of the

wintertime data which exhibit similar planetary scale flow patterns. This local, synoptic scale response to the mountain ranges resembles the *Day 1* systematic forecast error in the version of the ECMWF model that was operational before the introduction of envelope orography [Wallace et al. (1983)]. Hence, it appears that the performance of NWP models in the short term is dependent upon the accurate simulation of this local, synoptic scale response to the mountain ranges.

FIG.10. Climatological mean wintertime relative vorticity, averaged for the 850, 700 and 500mb levels, in units of 10^{-6} s^{-1}, negative contours are shaded. After Hsu (1986); as adapted from data in Lau et al., (1983).

(b) Influence of mountains on synoptic scale transients

By means of appropriate highpass filters, it is possible to isolate the spatial signatures of the synoptic scale transients associated with baroclinic waves. We have found that these signatures are not particularly sensitive to the choice of highpass filter; e.g., series of maps processed with Blackmon's (1976) 2.5-6 day period "bandpass filter" yields patterns very similar to 24 hour difference maps. In this section we will be showing lag correlations in maps processed with the nine point filter used by Lau and Lau (1984), which has a low frequency cutoff around 5 days.

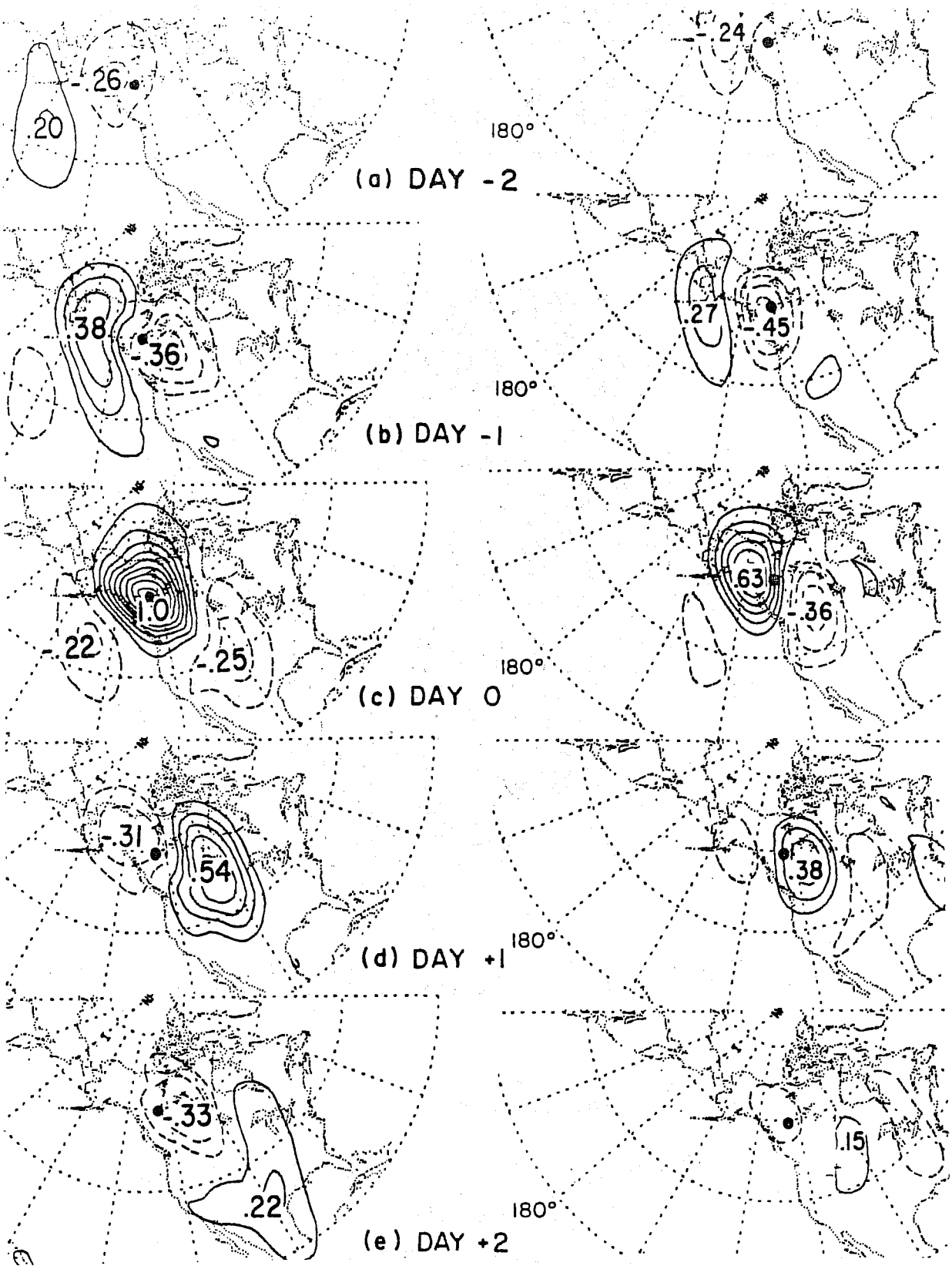

FIG.11. Lag correlation maps based on highpass filtered sea-level pressure at a gridpoint in the Yukon. The filter removes fluctuations with periods longer than about a week. Left panels are sea-level pressure charts, right panels are 500mb charts; contour interval 0.1, dashed contours denote negative correlations. Upper panels show hemispheric patterns 2 days in advance of the reference timeseries; middle panels show simultaneous correlations with the reference timeseries; and lower panels show hemispheric patterns 2 days later than the reference timeseries. After Hsu (1986).

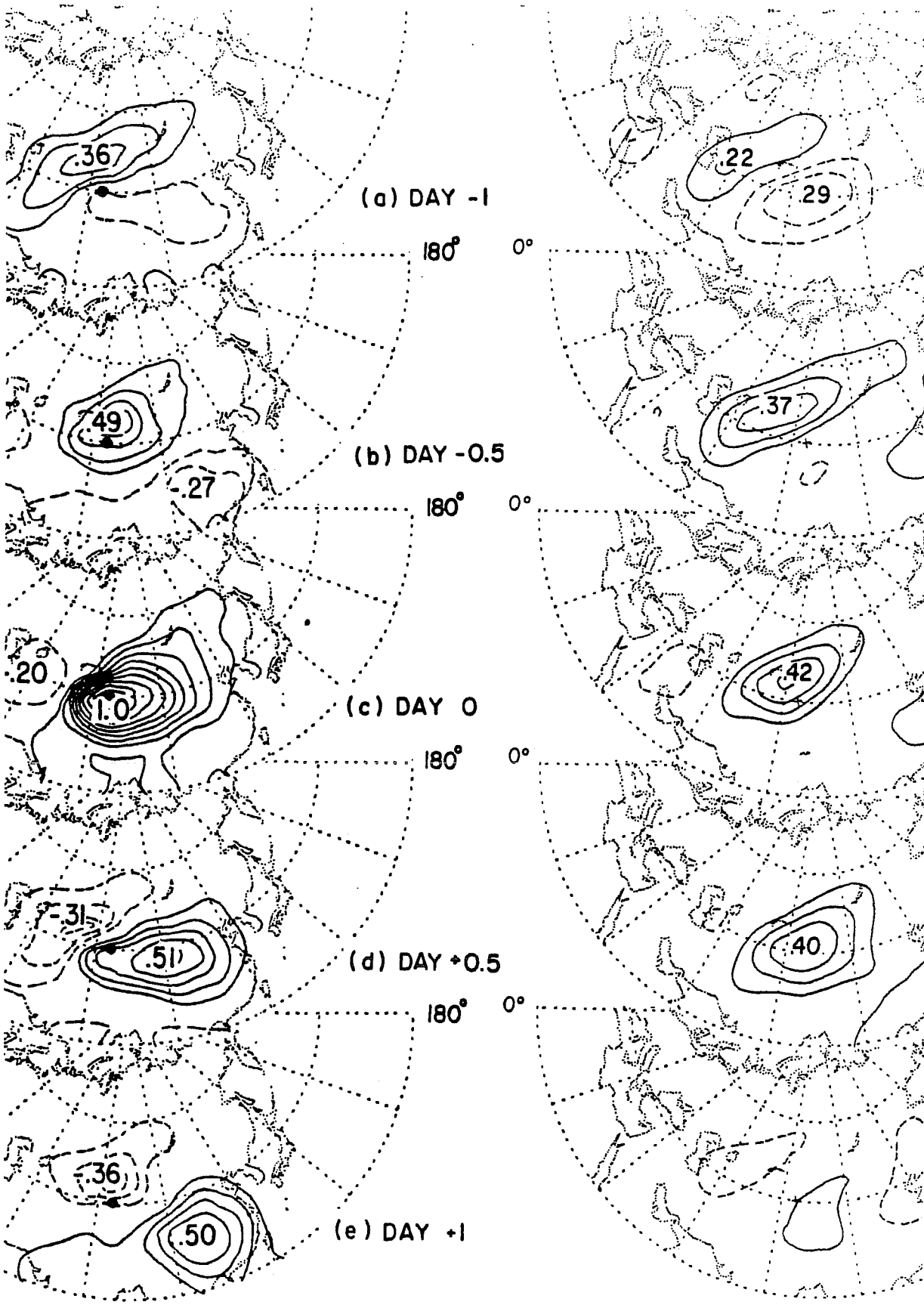

FIG.12. As in Fig.11, but for a gridpoint just to the north of the Tibetan Plateau. Note the shorter lag intervals

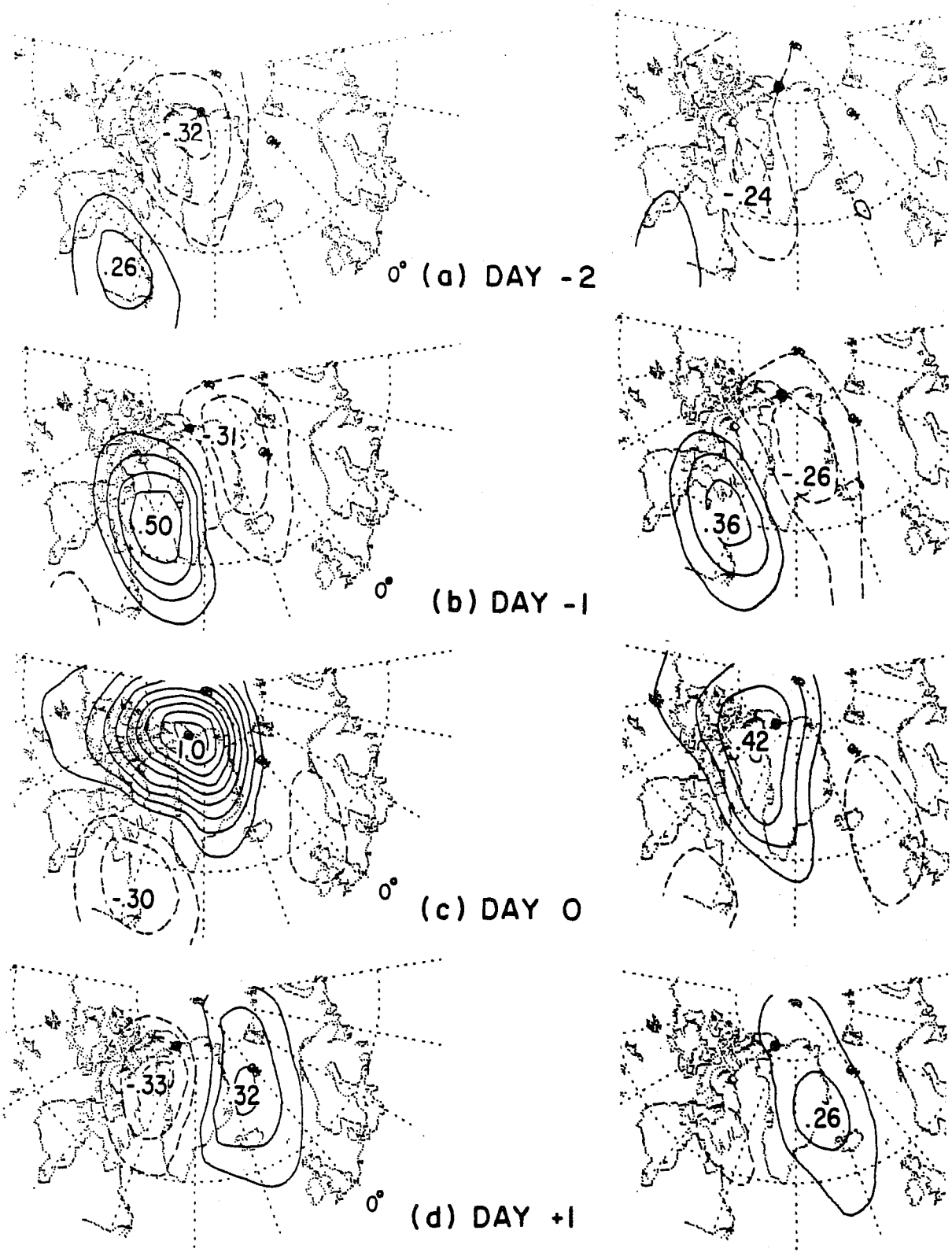

FIG.13. As in Fig.11, but for a gridpoint just to the north of Greenland.

Figs. 11-13 show sequences of lag-correlation maps based on highpass filtered sea-level pressure at gridpoints in the Yukon, just to the north of the Tibetan Plateau, and along the north coast of Greenland, respectively. As in the low-frequency results discussed above,

there is evidence of low-level phase propagation in the topographic waveguides. Hsu (1986) interprets this behaviour in terms of topographic Rossby waves propagating along shelves and/or escarpments, as discussed by Longuet-Higgins (1968a,b), Rhines (1969a,b, 1970), Mysak (1980) and others in the theoretical literature. We believe that the propagation of cyclones around South Africa, described by Gill (1977),is a reflection of the same phenomenon. It is interesting to note that the features propagating along these topographic waveguides are deformed in such a way as to be elongated in the along-slope direction. The corresponding features in the 500 mb height field tend to move more directly eastward than their counterparts in the SLP field. As a result of this differential motion at the two levels, baroclinic waves undergo some changes in vertical structure when they encounter mountain barriers. It is evident from Fig. 11 that systems crossing the Rockies tend to become more baroclinic in the leeward side, in agreement with previous case studies [Hess and Wagner (1948)] and with statistics on the local correlation between 1000 and 500 mb height in the high frequency fluctuations [Blackmon et al. (1979)]. However, the transformation in vertical structure is not as radical as in the case of the low frequency, planetary scale fluctuations discussed in the previous section.

In the synoptic climatology literature, a distinction is usually made between the tracks of cyclones and anticyclones in the SLP field [e.g., see Petterssen (1956), Klein (1957), Reitan (1971), Whittaker and Horn (1984)]. From these and other works on the climatological mean stormtracks one obtains the impression that cyclone tracks tend, on average, to exhibit a poleward component, while anticyclone tracks exhibit an equatorward component. The latter is particularly evident in the case of cold air outbreaks along the lee slopes of the major mountain ranges.

Fig.14 contrasts the movement of positive and negative SLP anomalies in the highpass filtered data based on composites for the Yukon gridpoint. The positive anomalies appear to be steered a little more strongly by the mountains, but the two composites are much more similar than one might have anticipated on the basis of the previous literature. Analogous composites for the same two sets of calendar dates, but based on data that are unfiltered except for the removal of a least squares best fit parabola for each of the 22 individual winter seasons in the sample, are shown in Fig.15. Again, the positive and negative composites are remarkably similar.

In order to reconcile the behaviour illustrated in Figs. 14 and 15 with the observed differences between cyclone and anticyclone tracks one must conclude that the apparent movement of highs and lows depends as much as upon the background climatological mean SLP field as upon the movement of pressure perturbations. As evidence in support of this assertion, Fig.16 shows the actual composite SLP charts for exactly the same two sets of

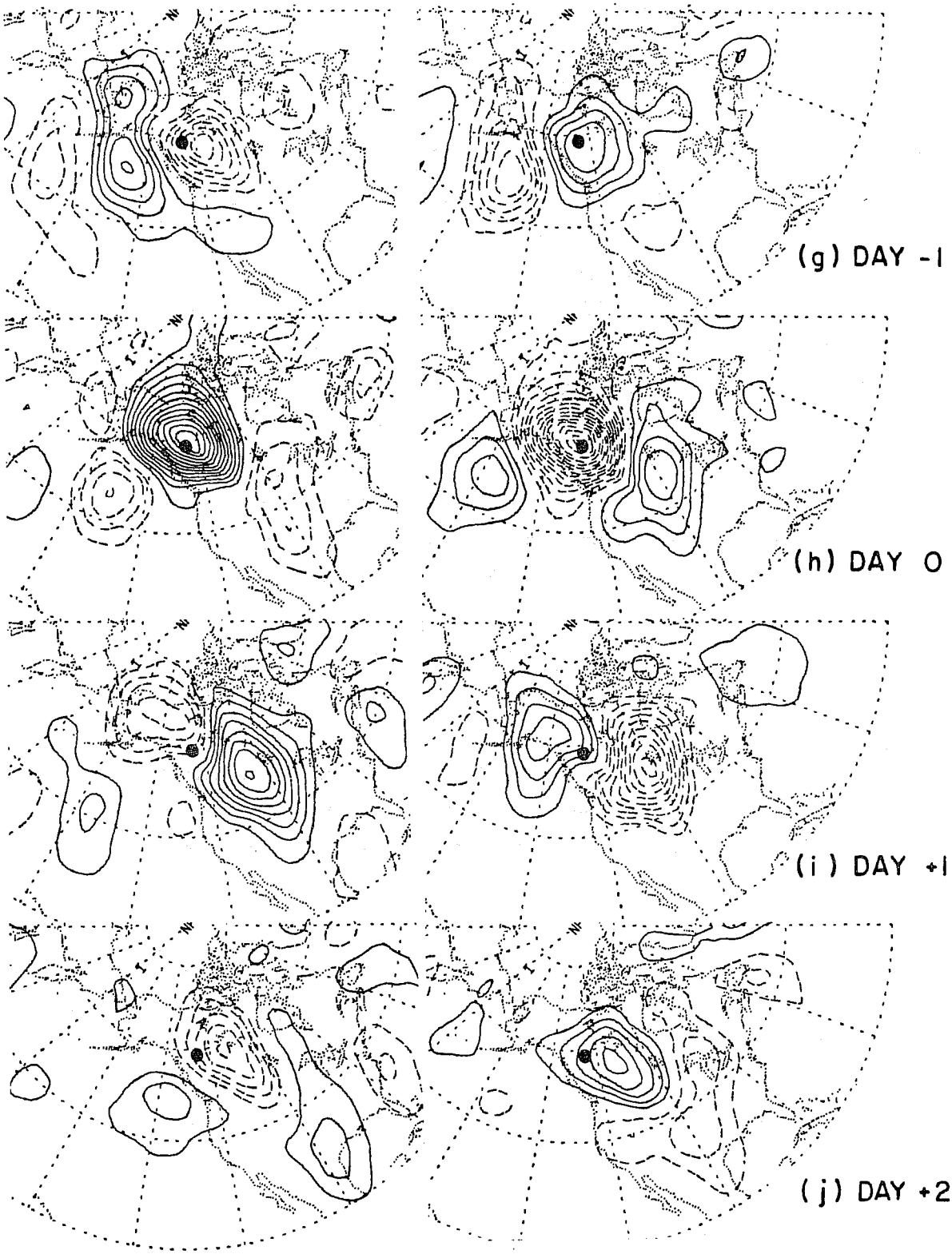

FIG.14. Composite sea-level pressure anomaly charts based on highpass filtered sea-level pressure at a gridpoint in the Yukon. The filter removes fluctuations with periods longer than about a week. Left panels are for positive anomalies at the reference gridpoint; right panels for negative anomalies. Upper panels show hemispheric patterns 2 days in advance of large pressure anomalies at the reference gridpoint; middle panels show patterns concurrent with large pressure anomalies at the reference gridpoint; and lower panels show hemispheric patterns 2 days later. Contour interval mb. The zero contour is omitted. Dashed contours denote negative anomalies. After Hsu (1986).

dates as in the previous two figures. The positive composite is dominated by the southeastward movement of the cold anticyclone in the lee of the Rockies, while in the latter, ones' attention is drawn to the quasistationary cyclone along the coast of British Columbia, which first intensifies and subsequently fills. The intensification is associated with a deepening, northeastward moving trough of low pressure in the westerlies on *Day -1* (not shown) which is absorbed into the primary low pressure area on *Day 0*. Hence, the synoptic charts are not inconsistent with the notion that anticyclones move southeastward while cyclones move northeastward. Upon closer inspection one can see a trough of low pressure moving

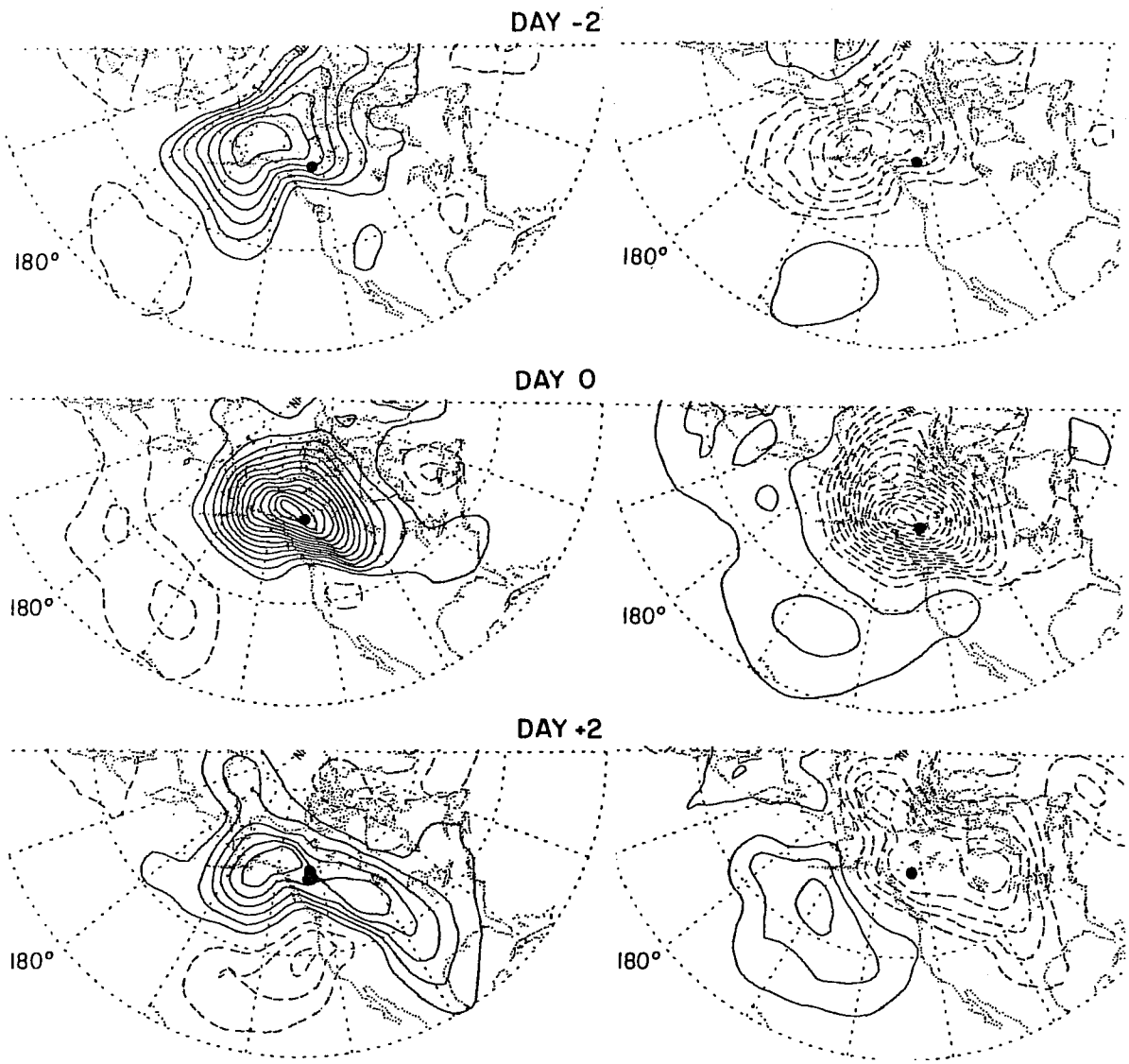

FIG.15. Composite sea-level pressure anomaly charts for the same dates and times as in the previous figure, but in this figure the "anomalies" plotted on the maps are deviations from the seasonally adjusted climatological mean [as defined by the least squares best fit parabola, fitted separately for each individual winter season] rather than highpass filtered anomalies. Left panels are for positive anomalies at the reference gridpoint; right panels for negative anomalies. Upper panels show hemispheric patterns 2 days in advance of large highpass filtered pressure anomalies at the reference gridpoint; middle panels show patterns concurrent with large highpass filtered pressure anomalies at the reference gridpoint; and lower panels show hemispheric patterns 2 days later. Contour interval 2mb. The zero contour is omitted. Dashed contours denote negative anomalies. After Hsu (1986).

southeastward across and in the lee of the Rockies, but this feature is rather subtle and easily missed in the raw synoptic charts. The difference between Figs.15 and 16, which convey such different impressions, is simply the background climatology shown in Fig.17.

That positive and negative anomalies in the SLP field should behave in such a similar manner implies that the dynamical processes responsible for the steering of low level circulation features in topographic waveguides are rather linear. Hsu (1986) argues that the strong static stability is responsible for restricting this steering effect to the lower troposphere. Though the large temperature perturbations associated with these synoptic scale systems influence the static stability, Hsu (1986) shows that the modulation is only on the order of 20% of the mean static stability in these regions. If potential vorticity is conserved in these systems, the relative changes in absolute vorticity should be of the same order. Hence, it is not surprising that the behavior of these systems should appear linear, to first order.

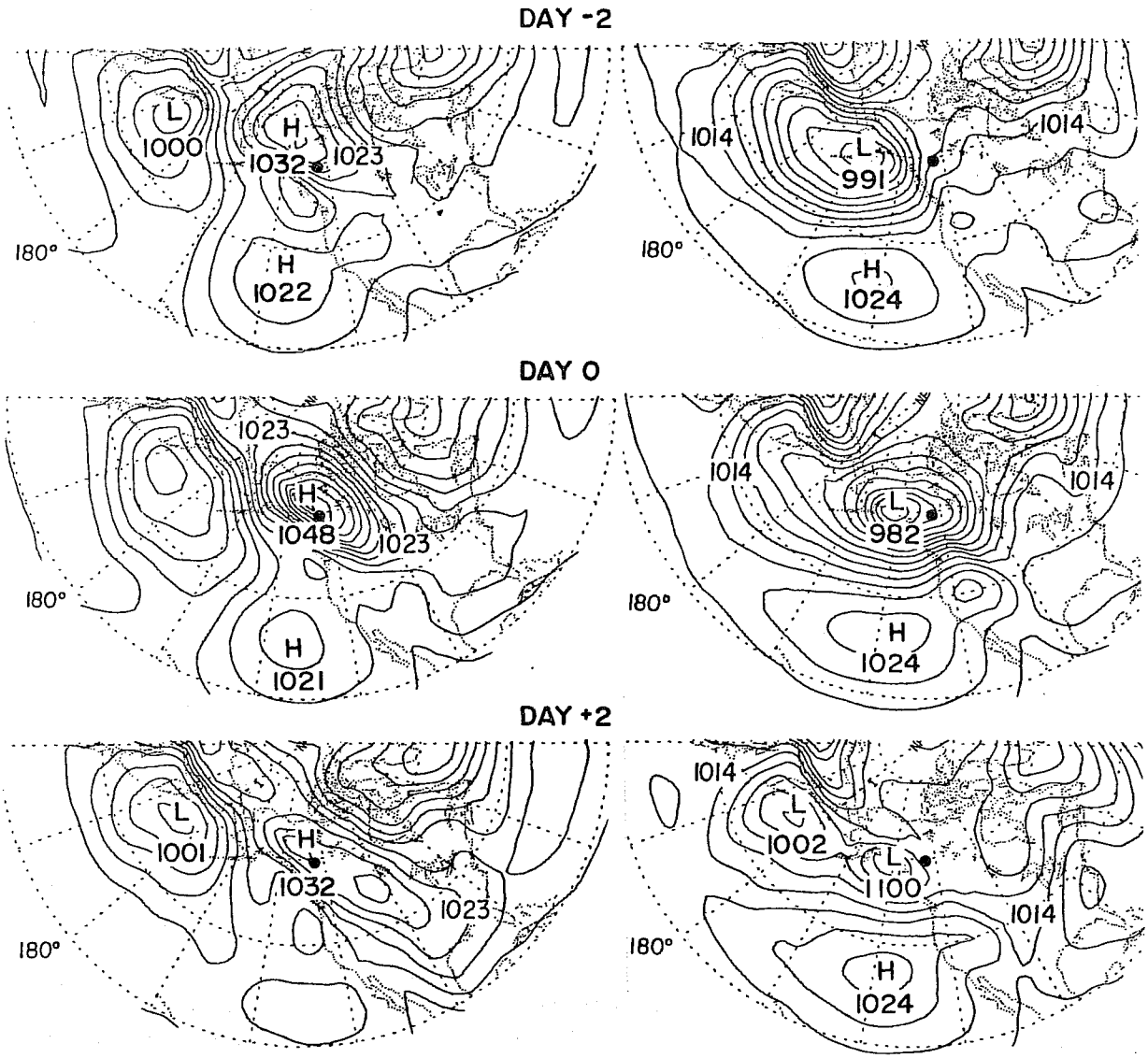

FIG.16. Composite sea-level pressure charts for the same dates and times as in the previous two figures. Contour interval 3 mb. After Hsu (1986).

The above examples illustrate that many of the synoptic-scale phenomena in the vicinity of mountain ranges, which appear to be quite complex in terms of structure and evolution, can be understood in terms of the superposition of (1) a background climatology, rich in planetary and synoptic scale structures induced by mountains and land/sea contrasts, and (2) moving baroclinic waves steered and deformed by the mountains in a rather simple manner.

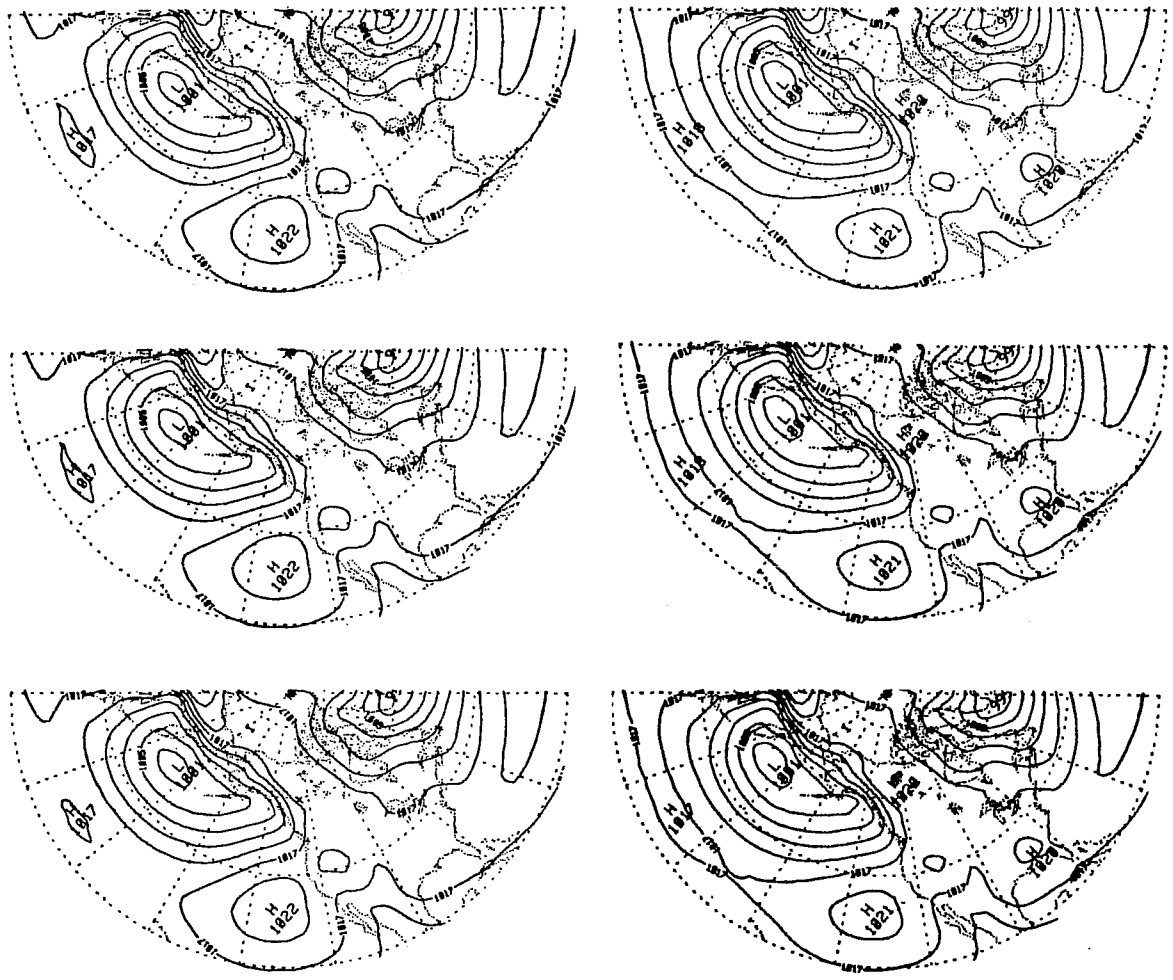

FIG.17. Difference between the patterns in the previous two figures; i.e., the seasonally adjusted climatological mean [as defined by the least squares best fit parabola, fitted separately for each individual winter season] for the calendar dates and times of the composites in Figs.14-16. Contour interval3mb.

Fig.18 provides a hemispheric survey of the effects of mountains in steering synoptic scale SLP fluctuations. It was generated in the following manner. On the basis of highpass filtered lag- correlation maps analogous to these in Figs.12-14, it is possible to define a "phase velocity" vector which represents the movement of the positive "centre of action" in the vicinity of the base gridpoint. Formally this is done by dividing the vectorial distance

phase velocity. Since the 500 mb phase velocity vectors were shown by Blackmon et al. (1984) to be closely related to the 700mb wind field which is the effective "steering flow" for baroclinic waves in the linear theory, the differential phase velocity between the 1000 and 500mb levels may be interpreted as the steering of the low circulation features by the terrain. The pattern Fig.18 is dominated by a general poleward movement of features in the SLP field relative to those in the 500mb height field, which we associate with the occlusion process. However, there is clear evidence of anticyclonic steering of low level circulation features around the major terrain features, as illustrated in the accompanying schematic.

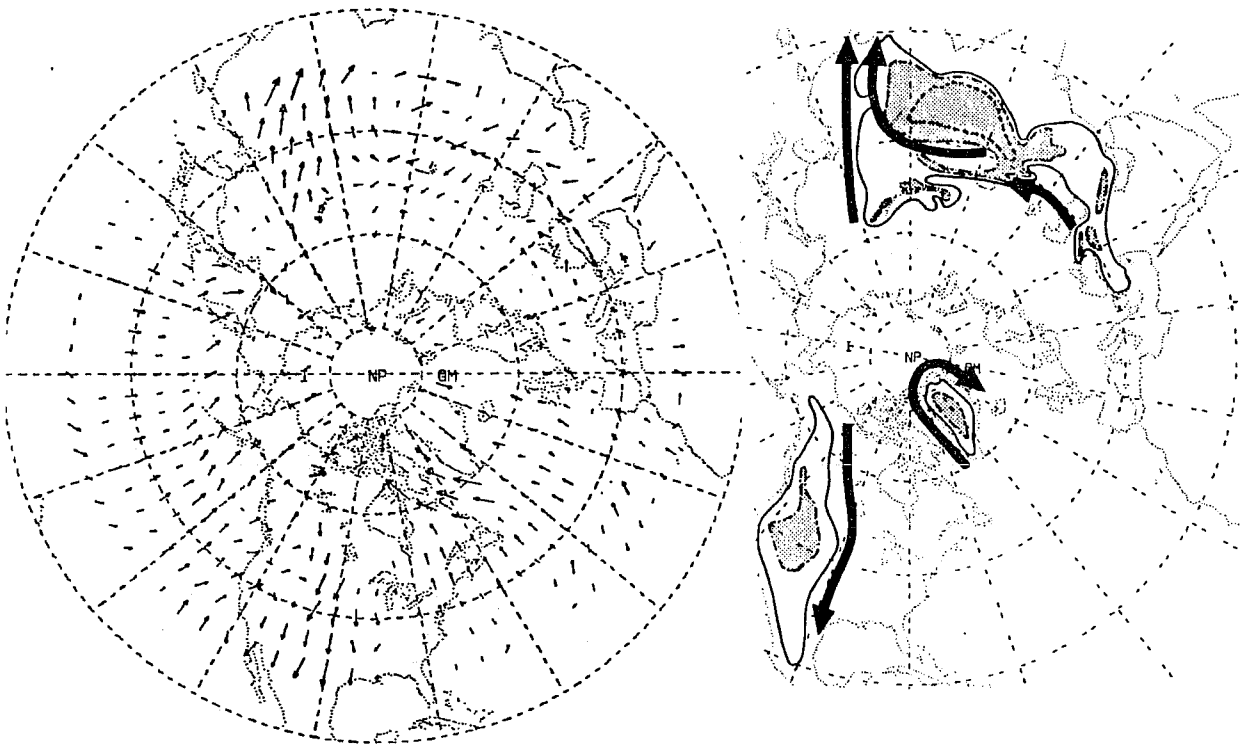

FIG.18. Difference between the phase velocity of synoptic scale features in the sea-level pressure and 500mb height fields during winter, as inferred from the movements of centres of action on lag correlation charts based on highpass filtered data. The method of calculation is described in the text.

In one of the first formulations of a two-level, dynamical weather prediction model, Reed (1958) assumed that dynamical processes at the 500 mb level could be represented by the nondivergent barotropic vorticity equation, while his prognostic equation for the 1000 mb height field allowed for the possibility of baroclinic structures in the 1000/500 mb layer which could arise as a result of a number of different processes, including the equivalent beta effect associated with the terrain slope. His model explicitly includes a term in the effective "steering flow" for the 1000 mb potential vorticity field which has the effect of advecting features along the contours of constant surface elevation. This effect is, of course, implicit in today's much more sophisticated multi-layer models.

5. Subsynoptic scale features

With the horizontal resolution of the most advanced numerical prediction models now approaching 100km and likely to increase further within the next decade, the numerical modeling of orographic effects on the subsynoptic (80-200km for the purposes of this discussion) takes on major importance. A detailed discussion of these effects is beyond the scope of this lecture, but a few rather general comments are perhaps in order.

The influence of orography is more pervasive and more complex on the subsynoptic scale than on the larger scales considered in the previous sections. The large ranges, such as the Himalayas and Rockies,assume much greater complexity as their various subranges begin to come into focus in the higher resolution models. The Alps, which are virtually invisible on the planetary scale and exert only a modest influence on the synoptic scale, assume the proportions of a major orographic barrier on the subsynoptic scale; and smaller ranges such as the Appenines and the Pyrenees emerge as important orographic features. Even the subtle orographic features of the British Isles leave their signatures on the subsynoptic scale climatology through their influence on convective precipitation.

In contrast to the large scale atmospheric response to orography, which appears to be dominated by linear Rossby wave dynamics, the subsynoptic scale response is likely to be more complex, with Kelvin (or edge) waves and nonlinear process (as manifested in phenomena such as density currents) playing an increasingly important role as resolution increases. [In this respect, Hsu (1986) has noted that the 40 m/s phase speed and the short meridional scale of the wave propagating along the northern edge of the Tibetan Plateau in Fig.12 from *Day 0* to *Day 0.5* is not incompatible with the dispersion relation for Kelvin waves.] The diurnal cycle is likely to play an important role in the subsynoptic scale response, particularly during summer.

Since the World Weather Watch network does not resolve the subsynoptic scale structures induced by mountains, it is necessary to rely upon the models to provide the context for interpreting the widely spaced observations over mountainous terrain. Hence, it is inevitable that subsynoptic scale structures in correlation maps analogous to those shown in the previous sections will be strongly model dependent. Nevertheless, correlation maps analogous to those shown in the previous section, but for fields with higher spatial and temporal resolution, should be quite instructive.

REFERENCES

Benzi, R., P. Malguzzi, A. Speranza and A. Sutera, 1986: The statistical properties of the general circulation: observational evidence on a minimal theory of bimodality. *Quart. J. R. Met. Soc.*, **112**, 661-676.

Blackmon, M.L., 1976: A climatological spectral study of the 500mb goepotential height of the Northern Hemisphere. *J. Atmos. Sci.*, **33**, 1607-1623.

Blackmon, M.L., R.A. Madden, J.M. Wallace and D.S. Gutzler, 1979: Geographical variations in the vertical structure of geopotential height fluctuations. *J. Atmos. Sci.*, **36**, 2450-2466.

Blackmon, M.L., Y.-H. Lee, J.M. Wallace, and H.-H. Hsu, 1984b: Time evolution of 500mb height fluctuations with long, intermediate, and short time scales as deduced from lag-correlation statistics. *J. Atmos. Sci.*, **41**, 981-991.

____, and Lau N.-C., 1980: Regional characteristics of the Northern Hemisphere winter circulation: A comparison of a simulation of a GFDL general circulation model with observations. *J. Atmos. Sci.*, **37**, 497-514.

Bolin, B., 1950: On the influence of the Earth's orography on the general circulation of the westerlies. *Tellus*, **2**, 184-195.

Charney, J.G., and J.G. Devore, 1979: Multiple flow equilibria in the atmosphere and blocking. *J. Atmos. Sci.*, **36**, 1205-1216.

____, and P.G Drazin, 1961: Propagation of planetary scale disturbances from the lower into the upper atmosphere. *J. Geophys. Res.*, **66**, 83-109.

____, and A. Elliassen, 1949: A numerical method for predicting the perturbation of the midlatitude westerlies. *Tellus*, **1**, 38-54.

Crutcher, H.L. and J.M. Meserve, 1970: Selected level heights, temperatures and dew points for the Northern Hemisphere, NAVAIR 50-1C-52 rev., Naval Oper., Washington, D.C., 1970.

Gill, A.E., 1977: Coastally trapped waves in the atmosphere. *Quart. J. Meteor. Soc.*, **103**, 431-440.

Grose, W.L., and B.J. Hoskins, 1979: On the influence of orography on large-scale atmospheric flow. *J. Atmos. Sci.*, **36**, 223-234.

Hansen, A., 1986: Observational characteristics of atmospheric planetary waves with bimodal amplitude distributions. *Adv. in Geophys.*,

Held, I.M., 1983: *Theory of stationary eddies. In Large-scale dynamical processes in the atmosphere*, B.J. Hoskins and R. Pearce, eds., Academic Press. 127-168.

Hess, S. and H. Wagner, 1948: Atmospheric waves in the northwestern United States. *J. Meteor.*, **5**, 1-19.

Hsu, H.-H., 1986: On the propagation of low-level circulation features in the vicinity of mountain ranges. Submitted to *J. Atmos Sci.*

____, and J.M.Wallace, 1985: Vertical structure of wintertime teleconnection patterns. *J. Atmos. Sci.*, **42**, 1694-1710.

Klein, W.H., 1957: Principal tracks and mean frequencies of cyclones and anticyclones in the Northern Hemisphere. Res. Paper No. 40, U.S. Weather Bureau, U.S. Gov't Printing Office, Washington, D.C.

Lau, N.-C., G.H.White and R.L. Jenne, 1981: Circulation statistics for the extratropical Northern Hemisphere based on NMC analyses. NCAR Technical Note. 138pp.

____, and K.-M. Lau, 1984: The structure and energetics of midlatitude disturbances accompanying cold-air outbreaks over East Asia. *Mon. Wea. Rev.*, **112**, 1309-1327.

Longuet-Higgins, M.S., 1968a: On the trapping of waves along a discontinuity of depth in a rotating ocean. *J. Fluid Mech.*, **31**, 417-434.

____, 1968b: Double Kelvin waves with continuous depth profiles. *J. Fluid Mech.*, **34**, Part 1, 49-80.

Manabe, S., and T.B. Terpstra, 1974: The effects of mountains on the general circulation of the atmosphere as identified by numerical experiments. *J. Atmos. Sci.*, **31**, 3-42.

Mysak, L.A., 1980: Recent advances in shelf wave dynamics. *Rev. Geophys. Space Phys.*, **18**, 211-241.

Newton, C.W., 1971: Mountain torques in the global angular momentum balance. *J. Atmos. Sci.*, **28**, 623-628.

Oort, A.H., 1983: *Global Atmospheric Circulation Statistics, 1958-1973*. NOAA Professional Paper 14.

Palmer, T.N., G.J. Shutts, and R. Swinbank, 1986: Alleviation of a systematic westerly bias in the general circulation and numerical weather prediction models through an orographic gravity wave drag parameterization. *Submitted for publication.*

Petterssen, S., 1956: *Weather Analysis and Forecasting, Vol.1*, Second Edition. McGraw-Hill, New York, 428pp.

Reed, R.J., 1958: A graphical prediction model incorporating a form of nonadiabatic heating. *J. Meteor.*, **15**, 1-8.

Reitan, C.H., 1974: Frequencies of cyclones and cyclogenesis for North America, 1951-70. *Mon. Wea. Rev.*, **102**, 861-868.

Rhines, P.B.,1969a: Slow oscillations in an ocean of varying depth.Part I. Abrupt topography. *J. Fluid Mech.*, **37**, 161-189.

____, 1969b: Slow oscillations in an ocean of varying depth. Part II. Islands and seamounts. *J. Fluid Mech.*, **37**, 191-205.

____,1970: Edge-, bottom-, and Rossby waves in a rotating stratified fluid. *Geophys. Fluid Dyn.*, **1**, 273-302.

Rossby, C.-G., 1939: Relations between variations in the intensity of the zonal circulation of the atmosphere and the displacement of the semipermanent centers of action. *J. Mar. Res.*, **2**, 38-55.

Starr, V.P., 1942: *Basic Principles of Weather Forecasting*. Harper Brothers, 299p.

Wallace, J.M., 1983: On the climatological mean statioary waves: observational evidence. *Large Scale Dynamics of the Atmosphere,* B.J. Hoskins and R.P. Pearce, eds., Academic Press, 27-54.

____, S. Tibaldi, and A.J. Simmons, 1983: Reduction of systematic forecast errors in the ECMWF model through the introduction of an envelope orography. *Quart. J. R. Met. Soc.,* **109**, 683-717.

Whittaker, L.M., and L.H. Horn, 1984: Northern Hemisphere extratropical cyclone activity for four mid-season months. *J. Climatol.*, **4**, 297-310.

Willet, H.C., 1944: *Descriptive Meteorology.* Academic Press, 310pp.